Multi-Center CDW-EIS description of the electron-impact ionization of aligned H_2 molecules.

E. Acebal* and S. Otranto
Instituto de Física del Sur (IFISUR), Departamento de Física, Universidad Nacional del Sur (UNS), CONICET, Av. L. N. Alem 1253, B8000CPB - Bahía Blanca, Argentina
(Dated: September 14, 2020)

In this work, the multi-center continuum distorted wave-eikonal initial state (MC-CDW-EIS) model is introduced. In contrast to previously reported CDW-EIS analyses for electron-molecule collisions, in which the ionized electron interacted with the molecular ion via a one-center effective potential, the multi-center nature of the molecular ion is explicitly taken into account. Results obtained for electron impact ionization of oriented H_2 molecules at the fully differential level are presented and contrasted to recent experimental data and to reported theoretical calculations obtained with the Time Dependent Close Coupling method. Present results suggest that this simple molecule still represents a challenging target from the theoretical point of view and that many aspects of the ionization process at the fully differential level remain to be understood.

I. INTRODUCTION

The electron-impact ionization of atoms and molecules has represented a challenging field for decades [1–3]. While a large fraction of these studies stemmed from the development of new experimental techniques, since the mid 1990s the introduction of reaction microscopes allowed for an unprecedented level of detail regarding collisions systems at the fully differential level. It is worth noting that this technique has not only been applied to the electron collisions field but in ion-impact and photon-impact studies as well [4–9]. Different laboratories worldwide adopted the technique since then [10–13]. These operating setups gave rise to large sets of data that have been useful to benchmark the existing theoretical models in different collisional processes.

From a theoretical point of view, we can distinguish the applied methods in two families: numerically intensive and perturbative treatments. While the former are nowadays considered capable to accurately reproduce the reported experimental cross sections at different collision geometries for simple atoms like H and He [14–16] and have been lately implemented for more complex atomic targets [17, 18], their extension to complex molecular targets is not so straightforward, even when the problem is simplified to a one electron treatment [19]. In contrast, distorted wave methods have proved to lead to acceptable results regarding simple targets like H, He and Ar [20–26], and can be in principle extended to deal with complex molecular targets at a considerably inferior computational cost. Such complex scenario has been mostly explored by means of variations of the distorted-wave-Born-Approximation (DWBA) [27–30] or variations of the 3C (sometimes termed BBK) model [31–33]. The post-collision interaction (PCI) among the projectile and the emitted electron at the wave function level was either neglected, or modelled by a simple multiplicative factor (such as the Gamow factor or the Ward-Macek factor [34]) that would not affect the computational cost in many of these calculations. Only recently, more elaborate DWBA models that explicitly incorporate the electron-electron interaction at all levels in the final state wave function have been introduced [27, 35].

In a previous work, we have implemented the CDW-EIS model for electron collisions with H_2O molecules [36]. This model has been largerly and successfully used to describe ion-atom collisions at intermediate to large impact energies [37–41] and to a much lesser extent in electron-atom collisions [21–25]. Compared to the Born initial state, the introduction of the eikonal initial state retains, in an asymptotic picture, the interaction of the projectile with the active electron and the molecular ion at the wavefunction level. In our case, we calculated fully differential cross sections for the single ionization of H_2O at an electron impact energy of 81 eV and found very good agreement with the reported experimental data for the denominated collision, semi-perpendicular and full-perpendicular planes [36]. In that work, the theoretical cross sections were properly averaged over the molecular orientation angles provided that the data were not orientation-resolved. Full account of the PCI at the wavefunction level was performed in this study.

In this work, we introduce a multi-center continuum-distorted wave-eikonal initial state model (MC-CDW-EIS) which in contrast to the usual CDW-EIS model, explicitly considers the multi-center nature of the recoiling molecular ion in the final state wave function. This model is benchmarked against the recent single ionization fully differential cross sections for $e^- + H_2$ collisions at the impact energy of 54 eV from Ren *et al.* [42] and other theoretical methods used to describe these data, such as the time-dependent close coupling (TDCC) [43]. We point out that this system is particularly relevant in our case, since the experimental studies have been carried out for oriented targets, thus providing a much more demanding test compared to other studies in which the

* emiliano.acebal@uns.edu.ar

molecular orientation is not resolved.

In the next section we describe the theoretical model. Results are discussed in section III, and the conclusions and outlook are drawn in section IV. Atomic units are used throughout this work unless otherwise stated.

II. THEORETICAL MODEL

Within this framework we analyse the $(e,2e)$ processes through the Gellman-Goldberger transition amplitude (T_{fi}), which is represented in its *post* version by

$$T_{fi} = \left\langle \Psi_f^- \left| W_f \right| \Psi_i^+ \right\rangle + \left\langle \Psi_f^- \left| V_i - W_f \right| \psi_i \right\rangle . \quad (1)$$

Here, ψ_i is the Born Initial State (BIS)

$$\psi_i = \frac{e^{i\mathbf{k}_0\cdot\mathbf{r}_1}}{(2\pi)^{3/2}}\varphi_i(\mathbf{r}_2) \quad (2)$$

and Ψ_i^+ is the Eikonal Initial State (EIS)

$$\Psi_i^+ = \frac{e^{i\mathbf{k}_0\cdot\mathbf{r}_1}}{(2\pi)^{3/2}}\varepsilon(\mathbf{r}_1)\,\varepsilon(\mathbf{r}_{12})\,\varphi_i(\mathbf{r}_2) \quad (3)$$

where $\varepsilon(\mathbf{r}_1)$ and $\varepsilon(\mathbf{r}_{12})$ are the eikonal phases

$$\begin{aligned} \varepsilon(\mathbf{r}_1) &= e^{-\frac{iZ}{k_0}\ln(k_0 r_1 - \mathbf{k}_0\cdot\mathbf{r}_1)} \\ \varepsilon(\mathbf{r}_{12}) &= e^{\frac{i}{k_0}\ln(k_0 r_{12} - \mathbf{k}_0\cdot\mathbf{r}_{12})} \end{aligned} \quad (4)$$

solutions to the Coulomb potentials in the asymptotic limit between the projectile and a single center of charge $Z=1$ and the active electron respectively, as described in previous works [36, 44]. We define $\mathbf{k}_0$ as the impinging electron momentum, $\mathbf{r}_1$ and $\mathbf{r}_2$ are the positions of the projectile and the active electron respectively and $\mathbf{r}_{12} = \mathbf{r}_1 - \mathbf{r}_2$. In this work, the molecular orbital wave function $\varphi_i(\mathbf{r}_2)$ was calculated by means of the linear combination of atomic orbitals (LCAO) approximation

$$\varphi_i(\mathbf{r}_2) = \sum_{m=1}^{N_{AO}} C_m \varphi'_m(\mathbf{r}_2). \quad (5)$$

N_{AO} is the number of atomic orbitals $\varphi'_m(\mathbf{r}_2)$ used, which were expanded by the 3-21G basis set and the coefficients C_m for the molecular orbital were determined by a self-consistent field calculation performed by the GAMESS quantum chemistry package [45].

The initial-state perturbation V_i in Eq. (1) is equal to $V_i = -Z/r_1 + 1/r_{12}$. The final perturbation operator W_f is obtained from the Schrödinger equation $(H-E)\,\Psi_f^- = W_f \Psi_f^-$ and is equal to $W_f = \nabla_{\mathbf{r}_1}\cdot\nabla_{\mathbf{r}_{12}} - \nabla_{\mathbf{r}_2}\cdot\nabla_{\mathbf{r}_{12}}$. The final state wave function represents two electrons in the continuum of the molecular ion and is given by

$$\begin{aligned} \Psi_f^- =& \chi^-(\mathbf{k}_1,\mathbf{r}_1)\,\chi^-(\mathbf{k}_2,\mathbf{r}_2) \\ & \times N^-(\alpha_3)\,{}_1F_1(i\alpha_3, 1, -ik_{12}r_{12} - i\mathbf{k}_{12}\cdot\mathbf{r}_{12}). \end{aligned} \quad (6)$$

Here, $\mathbf{k}_1 = \sqrt{2E_1}$ and $\mathbf{k}_2 = \sqrt{2E_2}$ are the scattered projectile and emitted electron final momenta, respectively, being E_1 and E_2 their emitted energies, $\mathbf{k}_{12} = (\mathbf{k}_1 - \mathbf{k}_2)/2$, $\alpha_3 = 1/(2k_{12})$ is the Sommerfeld parameter for the electron-electron interaction and $N^-(\alpha_3) = e^{\pi/2\alpha_3}\Gamma(1-i\alpha_3)$. The post-collisional interaction is represented by the confluent hypergeometric function, solution to the Coulomb potential between the pair of electrons. The distorted waves $\chi^-(\mathbf{k}_i,\mathbf{r}_i)$ take into account the interaction of the projectile and emitted electron with the molecular ionic core via the potential

$$\begin{aligned} V_{ion}(\mathbf{r}_i) &= \overbrace{V^{e-N}(\mathbf{r}_i)}^{} + \overbrace{V^{e-e}(\mathbf{r}_i)}^{} \\ &= \overbrace{-\sum_{j=1}^{N}\frac{Z_j}{R_{ij}}}^{} + \overbrace{\sum_{n=1}^{N_{MO}} N_e \int d^3\mathbf{r}' \frac{|\varphi_n(\mathbf{r}')|^2}{|\mathbf{r}_i - \mathbf{r}'|}}^{}. \end{aligned} \quad (7)$$

Here, the first sum V^{e-N} represents the particles interactions with the N nuclei of the molecule, where Z_j are the different atomic numbers corresponding to each nuclei and R_{ij} is the modulus of the vector $\mathbf{R}_{ij} = \mathbf{r}_i - \mathbf{R}_j$, being $\mathbf{R}_j$ the position of each nueclei with respect to the ion center of mass. The second sum V^{e-e} of Eq. (7) stands for the particles interactions with the ion-remaining electrons. N_{MO} is the number of molecular orbitals, $|\varphi_n(\mathbf{r}')|^2$ are the different electron densities corresponding to each orbital and N_e is the number of electrons present in the n-th orbital. In this work, for the wave function $\varphi_n(\mathbf{r}')$ we make use of the molecular orbital of H_2 calculated for the initial state $\varphi_i(\mathbf{r_2})$. We performed a calculation of V_{ion} considering the eigenstate of the molecular ion H_2^+ for $\varphi_n(\mathbf{r}')$ and no significant differences were observed. In addition, we decided to fix the modulus of $\mathbf{R}_j$ at 0.55 *a.u.* in order to mimic the experimental conditions from Ref. [42].

It can be seen from Eq. (7) that the anisotropy of $V_{ion}(\mathbf{r}_i)$ can be difficult to take into account, in particular for perturbative methods. In this sense, in its simplest form the CDW-EIS model completely neglects the multi-center nature of the residual ion by considering it as a single center with effective charge Z (Belkic's charge $Z = \sqrt{2n^2|\epsilon_i|}$ has been a frequent choice in the ion-atom context [41], where ϵ_i represents the ionization energy of the i-th orbital). In this case, the distorted waves $\chi^-(\mathbf{k}_i,\mathbf{r}_i)$ are just described by Coulomb functions

$$\begin{aligned} C^-(\mathbf{k}_i,\mathbf{r}_i) =& \frac{e^{i\mathbf{k}_i\cdot\mathbf{r}_i}}{(2\pi)^{3/2}} N^-(\alpha_i) \\ & \times {}_1F_1(i\alpha_i, 1, -ik_i r_i - i\mathbf{k}_i\cdot\mathbf{r}_i), \end{aligned} \quad (8)$$

eigenstates of the potential $V_{1C}(r_i) = -Z/r_i$.

Despite its simplicity regarding the molecular ion description, the CDW-EIS model was employed with success to describe the ionization of H_2O by electron impact in energetic asymmetrical emission conditions [36]. In that work, the molecular ion was considered in the final

state as a single center of charge $Z = 1$ and led to good agreement with the reported data. Nevertheless, a more robust and straightforward approach which incorporates the anisotropy of the residual ion is desirable, specially to study ionization processes at low impact energies and for energetically symmetric emissions.

A first approximation can be to spherically average the anisotropic potential $V_{ion}(\mathbf{r}_i)$ to obtain

$$U(r_i) = \frac{1}{4\pi}\int d\Omega\, V_{ion}(\mathbf{r}_i)\,. \tag{9}$$

Although the implementation of this average procedure provides an isotropic description of the molecular ion, the main advantage relies on the fact that the distorted waves $\chi^-(\mathbf{k}_i, \mathbf{r}_i)$ can be separated in a radial and an angular part with respect to only one center,

$$\chi^-(\mathbf{k}_i, \mathbf{r}_i) = \sum_{l=0}^{\infty} \frac{(2l+1)}{k_i r_i} i^l e^{-i\sigma_l} u_l(k_i, r_i)\, P_l(\hat{k}_i \cdot \hat{r}_i), \tag{10}$$

where $\sigma_l = \sigma_l^{Coul} + \delta_l$, $\sigma_l^{Coul} = \arg[\Gamma(l+1+i\alpha_i)]$, δ_l is the non-Coulombic phase shift of the radial waves ($\delta_l = 0$ for the Coulomb radial waves) and $P_l(\hat{k}_i \cdot \hat{r}_i)$ are the Legendre polynomials. The radial wave function $u_l(k_i, r_i)$ satisfies the equation

$$\left[-\frac{1}{2}\frac{d^2}{dr_i^2} + \frac{l(l+1)}{2r_i^2} + U(r_i)\right] u_l(k_i, r_i) = \frac{k_i^2}{2} u_l(k_i, r_i)\,. \tag{11}$$

This approximation was employed in previous works on ion-CH_4 and ion-H_2O obtaining good overall agreement with the experimental data [46, 47].

Previous approaches presented by Chuluunbatar and co-workers [32, 33] neglect the second sum in Eq. (7) to obtain

$$V^{e-N}(\mathbf{r}_i) = -\sum_{j=1}^{N} \frac{Z_j}{R_{ij}} \tag{12}$$

By doing so, the molecular anisotropy information is retained at the potential level, neglecting any spatial detail on the repulsive ion-remaining electrons interaction besides charge screening. The approximated distorted wave function for the final state, then consists in the product of Coulomb functions,

$$\begin{aligned}\chi^-(\mathbf{k}_i, \mathbf{r}_i) =& \frac{1}{(2\pi)^{3/2}} \prod_{j=1}^{N} e^{i\mathbf{k}_i \cdot \mathbf{R}_{ij}} N^-(\alpha_{ij}) \\ & \times {}_1F_1(i\alpha_{ij}, 1, -ik_i R_{ij} - i\mathbf{k}_i \cdot \mathbf{R}_{ij})\end{aligned} \tag{13}$$

In this approximation, effective charges Z_j need to be considered subjected to the condition that their sum leads to the asymptotic charge of the molecular ion ($Z = +1$ for single ionization). The Sommerfeld parameters α_{ij} take into account the interaction of electron i with respect to the atomic center j.

In this work we focus ourselves on preserving not only the molecular anisotropy but also the repulsive potential electron terms of Eq. (7), which provide information on the electron screening spatial dependence. In this sense, following a recent work on ion-H_2O multiple ionization collisions [48], we proceed by fitting $V_{ion}(\mathbf{r}_i)$ with the potential function:

$$\Phi(\mathbf{r}_i) = \sum_{j=1}^{N} \Phi_j(R_{ij}) = \sum_{j=1}^{N} -\frac{Z_j^{as} + Z_j^{in} e^{-a_j R_{ij}}}{R_{ij}} \tag{14}$$

Here Z_j^{as} represents the asymptotic charge of the atom j and Z_j^{in} is a correction factor in order that, at the vicinity of that atom, the continuum electrons feel a charge close to Z_j. The fitting parameters a_j control the charge decaying rate from $\left(Z_j^{as} + Z_j^{in}\right)$ to Z_j^{as}. The restriction $Z_1^{as} + Z_2^{as} + ... + Z_N^{as} = +1$ is imposed in order to reproduce the asymptotic charge of the molecular ion. It should be noted that with this fitting procedure no information from $V_{ion}(\mathbf{r}_i)$ is lost. Therefore, this method can be seen as a step forward in describing the ionization of multi-center targets. We call this approximation Multi-Center CDW-EIS (MC-CDW-EIS). In this work, and provided that the experimental data was collected for the ground state dissociation (GSD) channel only, we set $Z_1^{as} = 1$ and $Z_2^{as} = 0$. The parameters obtained for $\Phi(\mathbf{r}_i)$ are presented in Table I.

TABLE I. Fitting parameters obtained from $\Phi(\mathbf{r}_i)$ for H_2^+.

$H_{(j)}$	Z_j^{as}	Z_j^{in}	a_j
$H_{(1)}$	1	0	1
$H_{(2)}$	0	1.00	1.28

The ground state dissociation (GSD) is almost identical to nondissociative ionization since both processes involve vertical transitions without change of the internuclear distance [49]. The difference resides in the fact that GSD starts from smaller internuclear distances (1.1 *a.u.* for the ionization of H_2 in Ref. [42]) and populates continuum vibrational levels of the electronic ion ground state, which in the case of H_2^+ will subsequently fragment into a H atom and a proton. One of the advantages of studying this type of ionization is that the molecular orientation for a given ionization event can be determined from triple coincidence measurements between the two electrons and the proton, as reported in Ref. [42]. The energy conservation equation of this process can be written as

$$E_0 = E_1 + E_2 + Q \tag{15}$$

where E_0 is the impact energy and Q is the energy transferred to the target during ionization. This quantity contains information about the final vibrational level, though the energy resolution reported in Ref. [49] exceeds the energy spacing by about an order of magnitude.

The different potential approximations to $V_{ion}(\mathbf{r}_i)$ discussed so far are contrasted in Fig. 1 for an electron in the continuum of an H_2^+ ion aligned in the z axis. These are plotted along this axis as well. The effective charges considered for $V^{e-N}(\mathbf{r}_i)$ are $Z_1 = Z_2 = 0.5$.

Since $\Phi(\mathbf{r}_i)$ is a sum of different potentials, each one centered in a single atom, we approximate the final wavefunction as the product of the two-body solutions corresponding to each $\Phi_j(R_{ij})$

$$\begin{aligned}\chi^-(\mathbf{k}_i,\mathbf{r}_i) &= \prod_{j=1}^{N}\chi_j^-(\mathbf{k}_i,\mathbf{R}_{ij}) \\ &= \prod_{j=1}^{N}\left[\sum_{l=0}^{\infty}\frac{(2l+1)}{k_i R_{ij}} i^l e^{-i\sigma_{jl}} u_{jl}(k_i,R_{ij})\, P_l(\hat{k}_i\cdot\hat{R}_{ij})\right]\end{aligned} \tag{16}$$

The partial waves $u_{jl}(k_i,R_{ij})$ satisfy Eq. (11) with potential $\Phi_j(R_{ij})$ and, together with the non-Coulombic phase shifts δ_{jl}, can be obtained through Salvat's code [50]. Interestingly, these phase shifts become negligible as l increases, and due to the asymptotic limit of these potentials, the radial wave functions $u_{jl}(k_i,R_{ij})$ converge to the Coulombic ones $u_{jl}^{Coul}(k_i,R_{ij})$, which are solutions of Eq. (11) with potential $V(R_{ij}) = -Z_j^{as}/R_{ij}$. Of particular relevance in our case, is to analyse how the distorted wave solution of $\Phi_{(2)}$ differs from the free particle case ($Z_2^{as} = 0$). This can be seen in Fig. 2 where we consider an electron emitted with energies of 4 eV, 10 eV and 18 eV from the atomic center described by $\Phi_{(2)}$ and compare in each case its first two partial waves to those obtained for a free particle. It can be seen that the $l = 0$ partial wave is the most affected one and that at this emission energy a fast convergence towards the free particle partial waves is achieved. In our computer code, the different $\chi_j^-(\mathbf{k}_i,\mathbf{R}_{ij})$ are written as

$$\begin{aligned}\chi_j^-(\mathbf{k}_i,\mathbf{R}_{ij}) &= C^-(\mathbf{k}_i,\mathbf{R}_{ij}) + \sum_{l=0}^{L}\frac{(2l+1)}{k_i R_{ij}} i^l P_l(\hat{k}_i\cdot\hat{R}_{ij}) \\ &\times\left(e^{-i\sigma_{jl}} u_{jl}(k_i,R_{ij}) - e^{-i\sigma_{jl}^{Coul}} u_{jl}^{Coul}(k_i,R_{ij})\right).\end{aligned} \tag{17}$$

By doing so, the infinite partial waves can be accounted for by correcting from the asymptotic Coulomb wave function the partial waves for l-values lower than a certain L. The latter is determined by analysing the L-value from which the non-Coulombic phase shift δ_{jl} can be considered negligible thus reaching convergence. This strategy considerably reduces the numerical effort to be perfomed.

The calculation of the transition amplitude (T_{fi}) involves a 6 dimensional integration which was directly performed by the adaptive Vegas Monte Carlo algorithm [51]. The wave-packet approach of Malcherek and Briggs [52] was used, in order to treat the continuum-continuum transition. We estimate our numerical uncertainty to be less than 5%.

The fully differential cross section (FDCS) for the ionization of molecules by electron-impact as a function of the (T_{fi}) is given by

$$\begin{aligned}\frac{d^6\sigma}{dE d\Omega_1 d\Omega_2 d\alpha d\beta d\gamma} &= N_e (2\pi)^4 \frac{k_1 k_2}{k_0} \\ &\times\left[\frac{1}{4}\left|T_{fi}^D + T_{fi}^E\right|^2 + \frac{3}{4}\left|T_{fi}^D - T_{fi}^E\right|^2\right].\end{aligned} \tag{18}$$

Here, N_e is the number of electrons present in the molecular orbital to be ionized, T_{fi}^D and T_{fi}^E are the direct and exchange transition amplitudes, with $T_{fi}^E(\mathbf{k}_1,\mathbf{k}_2) = T_{fi}^D(\mathbf{k}_2,\mathbf{k}_1)$ and (α,β,γ) is the set of Euler angles which define the orientation of the molecular axes, following Landau convention [53]. For linear targets, such as H_2, the FDCS is invariant under γ rotations since these molecules have axial symmetry. The wave functions presented in Eq. (1) are defined in the molecular frame of reference. Therefore, in our calculations, we performed a rotation of these quantities by the set of Euler angles (α,β) to the laboratory frame in order to compute the transition amplitudes T_{fi}^D and T_{fi}^E.

The capture channel is not included in our one-active electron treatment for this collision system and its inclusion would require of a full 5-body treatment. To gain insight on the potential role of this channel we have performed classical trajectory Monte Carlo simulations in the context of a 5-body code succesfully employed to describe electron capture by ion impact at intermediate to low impact energies [54, 55]. These suggest that the influence of this channel is in the order of our numerical uncertainty. More work is currently under way in order to provide a quantitative assesment regarding this point.

III. RESULTS

In what follows we present the calculated fully differential cross sections (FDCS) for the single ionization of aligned H_2 molecules by electron-impact. These are benchmarked against the set of experimental data reported by Ren and co-workers [42] at the low impact energy of 54 eV and for different orientations of the molecular target for both equal- and unequal-emission energy sharing. In their setup one electron is scattered at $\theta_1 = -50°$ from the impinging projectile direction and the other is emitted perpendicular to this direction into the denominated perpendicular plane. Since these data are relative, a common factor was employed to normalize them to our theoretical results.

All these features (low impact energy, aligned targets, emission to the perpendicular plane and equal energy

sharing) play an important role in testing different theoretical methods. In this sense, we have performed calculations for three different approximations within the CDW-EIS formalism. In first place the residual ion is considered as a single center of charge $Z = +1$ leading to the well-known CDW-EIS model, which we will hereafter refer to as 1 Center (1C). Secondly, we employed the approximation V^{e-N}, which incorporates the multicenter nature of the target by neglecting the remaining-electron repulsive potential terms. Therefore, the residual ion is approximated by two centers with effective charges $Z_1 = 1$ and $Z_2 = 0$, since as it has been already mentioned that the experimental data is restricted to the ground-state dissociation (GSD) channel [42, 49], where H_2^+ dissociates into H^+ and H. We term this model 2 Center (2C). The third approximation considered is the multiple-center (MC) model introduced in the previous section. Considering that the specific location of H^+ and H for a particular molecular orientation is not reported, the theoretical curves presented are the average of two different FDCS with the asymptotic charges of $H_{(1)}$ and $H_{(2)}$ interchanged for a given orientation of the molecular axis.

First, in Fig. 3 we focus on the FDCS corresponding to both electrons being emitted with 18 eV for six different molecular orientations. In the top panel of Fig. 3 the molecular target is aligned along the z- and x-axes and therefore, symmetry considerations require structures to be symmetric around $\phi_2 = 0°$. For both cases the experimental data present a maximum along this direction, which corresponds to an electron being emitted in the x-axis direction. This obeys to the fact that the projectile momentum $\mathbf{k}_1$ lies in the $(-x)z$-quadrant of the collision plane, indicating a post-collisional interaction (PCI) effect. A narrower peak is observed in the case of x-axis alignment (Fig. 3(b)) suggesting a focusing mechanism along the molecular axis. No substantial differences are noted in these two cases between the theories hereby presented. From the comparison with the TDCC results from Ref. [42], we note that no theory provides perfect agreement with the data. For these two cases, the MC model is the one in better shape agreement with the data.

In the center and bottom panels of Fig. 3 the symmetry with respect to the xz plane is broken and a strong alignment dependence is observed in the experimental data. First, in Fig. 3(c) the molecular target is rotated 45° with respect to the z-axis from Fig. 3(b), and the experimental maximum is shifted following this molecular axis rotation. Here, the MC model correctly reproduces the peak position, while the 1C and 2C do not. A similar structure is observed in Fig. 3(d) where the molecular axis is tilted 45° from the xy plane, and the theories give analogous results with a slight decrease of magnitude presented by the MC model. With an additional rotation of 45° around the z-axis in Fig. 3(e), a more complicated experimental structure is found and the exhibited theories are in good overall agreement with it. In Fig. 3(f) a new 45° rotation around the z-axis is made. Except for this particular case, the MC model correctly reproduces the experimental peak position in contrast to the other theories. However, it should be pointed out that no perfect agreement is achieved by any of these models.

In Figs. 4 and 5, we analyse the FDCS as a function of the angle θ_{12} between the continuum electrons momenta $\mathbf{k}_1$ and $\mathbf{k}_2$, a representation to which not much attention has been paid so far for these data. Within the MC model we present the two calculated cross sections before the average procedure is performed, i.e., with the asymptotic charges of $H_{(1)}$ and $H_{(2)}$ interchanged. The dashed curves represent the case when the asymptotic charges of $H_{(1)}$ and $H_{(2)}$ are +1 and 0 respectively, while the solid curves stand for the opposite case. We also make the distinction when the proton lies inside or outside the cone of angle θ_{12} generated by the vectors $\mathbf{k}_1$ and $\mathbf{k}_2$ by means of blue and orange lines respectively. In this sense, we can gain insight on the possible role played by this proton on the receding electrons and its eventual responsibility for the unsymmetric patterns observed in Fig. 3 when the symmetry with respect to the xz plane is broken.

In the first column of Fig. 4 we study the molecular orientation defined by the pair of Euler angles ($\alpha = 45°, \beta = 90°$) where the target lies in the xy perpendicular plane and is rotated 45° from the x-axis around the z-axis, which corresponds to the case presented in Fig. 3(c). In Fig. 4(a), a graphical representation for the punctual case $\phi_2 = 0°$ is shown, together with the cone generated by $\mathbf{k}_1$ and $\mathbf{k}_2$ as they recede from the target. As $\mathbf{k}_2$ changes its direction along the xy plane, this cone changes its geometry and we find ϕ_2-ranges in which either $H_{(1)}$ or $H_{(2)}$ lie inside this cone. The lowest value of $\theta_{12} = 40°$ in Fig. 4(c) corresponds to the lowest value of $\phi_2 = -180°$ in Fig. 4(e). Therefore, increasing values of θ_{12} correspond to increasing values of ϕ_2, until θ_{12} reaches its highest value of $\theta_{12} = 140°$ which corresponds to $\phi_2 = 0°$. Following the curves in Fig. 4 (c), θ_{12} now decreases its value until it arrives again at $\theta_{12} = 40°$, which is equivalent to increasing ϕ_2 from 0° to 180° in Fig. 4(e). In Fig. 4(c) we observe a gap for the same values of θ_{12} within a single curve that accounts for the asymmetry observed in the bottom panel. When $H_{(2)}$ represents the proton (solid curve), we observe that the FDCS increases its magnitude when θ_{12} goes from 40° to 140°, which corresponds to the first half of the Fig. 4(e). When ϕ_2 goes from 6° to 45°, $H_{(2)}$ lies inside the cone generated by $\mathbf{k}_1$ and $\mathbf{k}_2$. Present results suggest that this emission geometry is responsible for the peak presented by the solid curve and the wide gap observed in the center panel. On the other hand, when $H_{(1)}$ has an asymptotic charge of +1 (dashed curve), this gap is almost negligible, since $H_{(1)}$ falls inside the cone for values of ϕ_2 between −135° and −35° which correspond to values of θ_{12} much lower than the previous case, indicating that the continuum electrons are emitted closer to each other. Therefore, the probability of emission into this region is disfavoured by the PCI, and so we observe a much wider structure in Fig. 4(e), without a maximum in the direc-

tion of $H_{(1)}$. This representation then provides a clue on why after the average procedure the maximum is shifted to higher values of ϕ_2 when the molecule is rotated 45° from Fig. 3(b) to Fig. 3(c) and is located around the direction of $H_{(2)}$, in agreement with the experimental data. In the right column of Fig. 4 the target alignment is defined by the pair of Euler angles ($\alpha = 45°, \beta = 45°$), and the results are very similar to the previous orientation considered, though in this case $H_{(1)}$ never falls inside the cone defined by θ_{12}. Then, we observe in Fig. 4(f) that both FDCS, with the asymptotic charges of $H_{(1)}$ and $H_{(2)}$ interchanged, give a maximum around the $H_{(2)}$ projection into the xy plane, and the contribution of considering $H_{(2)}$ as the proton seems to be dominant in the comparison with the experimental data.

For both cases of Fig. 4, Ren and co-workers [42] assumed that the emission to negative values of ϕ_2 was suppressed due to PCI effects. Present results support this statement. However, for the case shown in the first column of Fig. 5, where the molecular target lies in the yz plane, they expected that electron emission along the projections of the atoms $H_{(1)}$ and $H_{(2)}$ into the xy plane ($\phi_2 = \pm 90°$), should experience identical post-collisional interaction, but this was not the case. As it can be seen from Fig. 5(c) the gaps are still significant, so the pattern in Fig. 5(e) is not symmetric. We also observe that the gap of the solid curve is wider than for the dashed curve, since $H_{(2)}$ falls inside the cone defined by θ_{12} for high values of this angle. Besides, $H_{(1)}$ never falls inside the cone, so the gap is narrower and the relative magnitude between the two peaks exhibited in Fig. 5(e) for the case of considering $H_{(1)}$ as the proton is close to unity. From these results we are led to conclude that the emission for positive values of ϕ_2 is favoured due to a PCI effect affected by the orientation of the target atoms, as for the two cases presented in Fig. 4.

Finally, in the right column of Fig. 5 we study the molecular orientation defined by the pair of Euler angles ($\alpha = 135°, \beta = 45°$) where the target is rotated 45° around the z-axis, which corresponds to the case presented in Fig. 3(f). In this case, emission for positive values of ϕ_2 is still preferred. Nevertheless, the asymmetry shrinks down beacuse H_2 lies near the direction of $\mathbf{k}_1$. Consequently, the influence of H_2 when it falls inside the cone of angle θ_{12} is not enough to increase the FDCS magnitude for positive values of ϕ_2, since the continuum electrons are emitted closer to each other in comparison with the three previous cases. It can be seen in Fig. 5(d) that the gap for considering H_2 as a proton is narrower than for the dashed curve. Therefore, after the averaging procedure the MC model gives a preferential emission to negative values of ϕ_2, in disagreement with the experimental data.

This departure from the experimental FDCS structure raises the question of whether an averaging procedure for the theoretical model is the proper choice, since at this case H_2 is at the nearest position from the direction of $\mathbf{k}_1$, and therefore we can think that ionization events are most likely to occur when H_2 leaves the collision as a proton, hence making the solid curve dominant. However, this question remains unanswered at this point, since, as it was mentioned, the relative orientation of H^+ and H^0 for each ionizing collision event has not been reported.

In Fig. 6 we compare the FDCS obtained through the methods described above with the experimental and TDCC data for the molecular target aligned along the y-axis and three different electron emission energies. In the top panel of Fig. 6 an equal-energy emission of $E_1 = E_2 = 18$ eV is considered, where the experimental data present three different peaks. The first one lies among the x-axis direction ($\phi_2 = 0°$) and it seems to be a result of the PCI as explained for the two cases presented in the top panel of Fig. 3. The other two are shown at $\phi_2 = \pm 75°$, roughly along the molecular axis, indicating again a strong alignment dependence. While the TDCC results from Ref. [42] correctly describe the positions of the three peaks, we observe that the three theories presented here only predict two peaks in this case, which are in good agreement with the data but are not able to reproduce the third structure consisting in the x-axis direction maximum. We ascribe our subestimation of the central structure to the fact that the employed wavefunctions neglect the dynamical correlation among the different pairs or particles [56] in contrast to the TDCC method that includes such physical information explicitly.

In the center and bottom panels of Fig. 6, one electron emission energy is reduced from $E_2 = 18$ eV in (a) to $E_2 = 10$ eV in (b) and $E_2 = 4$ eV in (c). It can be seen that as the difference between the two electron energies $\Delta E = E_1 - E_2$ is increased, the two side peaks become dominant, and the x-axis direction maximum is decreased. Ren and co-workers concluded that this trend confirms the influence of the residual ion potential in the angular pattern exhibited by the continuum electrons. In these two other cases, neither of the three models presented here exhibit the $\phi_2 = 0°$ maximum, while the TDCC model correctly reproduce it as in the equal-energy sharing case. In addition, the MC model shows an increase of magnitude from Fig. 6(a) to Fig. 6(c) not exhibited in the experimental data nor in the other methods. A close inspection of Fig. 2, where the first two partial waves for an electron emitted with 18 eV, 10 eV and 4 eV from the atomic center described by $\Phi_{(2)}$ are presented, clearly shows that the $l = 0$ partial wave is responsible from the magnitude departure of MC from 2C in Figs. 6(b) and 6(c). A more accurate description of the ionized electron interaction with the molecular ion is clearly needed at this point, specially regarding the electron distribution in the H_2^+ ion in the field of the receding electrons.

IV. CONCLUSIONS

In this work, we have introduced the multi-center CDW-EIS model with the aim to provide an improved description of the final channel, with respect to the single center modellization, following the single ionization of anisotropic molecules.

We have evaluated its performance at the fully differential level in electron-H_2 collisions at low impact energies. This collision system was chosen due to the fact that orientation-resolved experimental data have been recently reported together with highly numerically intensive calculations, thus providing an ideal scenario to benchmark its performance.

Present results suggest that at present no theoretical method is capable of providing an accurate description of the reported data for the studied collision geometries. The numerical intensive TDCC method provides a good overall description of the relative magnitudes and shapes of the cross sections but discrepancies still remain with respect to peak positions and width of structures. In contrast, the MC-CDW-EIS model hereby introduced provides a good overall description of the peak positions and structures but fails to describe the relative magnitudes of the FDCS at different emission energies for the emitted electron. More experimental data for this particular target at different impact energies and emission geometries are welcome at this point, to provide assistance for future theoretical endeavours.

V. ACKNOWLEDGMENTS

Work at IFISUR supported by PGI/F073, Secretaría General de Ciencia y Tecnología, Universidad Nacional del Sur and PIP 11220170100855CO of CONICET, Argentina. We thank Dr. Xueguang Ren for providing us with the experimental data in tabular form.

[1] U. Amaldi Jr, A. Egidi, R. Marcoreno, and G. Pizzella, Rev. Sci. Instr. **40**, 1001 (1969).
[2] H. Ehrhardt, M. Schulz, T. Tekaat, adn K. Willmann, Phys. Rev. Lett. **22**, 89 (1969).
[3] H. Ehrhardt, K. Jung, G. Knoth, and P. Schlemmer, Z. Phys. D. **1**, 3 (1986).
[4] V. Mergel, R. Dörner, J. Ullrich, O. Jagutzki, S. Lencinas, S. Nüttgens, L. Spielberger, M. Unverzagt, C. L. Cocke, R. E. Olson, M. Schulz, U. Buck, E. Zanger, W. Theisinger, M. Isser, S. Geis, and H. Schmidt-Böcking, Phys. Rev. Lett. **74**, 2200 (1995).
[5] R. Dörner, V. Mergel, Liu Zhaoyuan, J. Ullrich, L. Spielberger, R. E. Olson, and H. Schmidt-Böcking, J. Phys. B: At. Mol. Opt. Phys. **28**, 435 (1995).
[6] R. Moshammer, M. Unverzagt, W. Schmitt, J. Ullrich, H. Schmidt-Böcking, Nucl. Instr. Methods Phys. Res. B **108**, 425 (1996).
[7] R. Dörner, H. Bräuning, J. M. Feagin, V. Mergel, O. Jagutzki, L. Spielberger, T. Vogt, H. Khemliche, M. H. Prior, J. Ullrich, C. L. Cocke, and H. Schmidt-Böcking, Phys. Rev. A **57**, 1074 (1998).
[8] J. Ullrich, R. Moshammer, A. Dorn, R. Dörner, L. Schmidt, and H. Schmidt-Böcking, Rep. Prog. Phys. **66**, 1463 (2003).
[9] T. Pflüger, O. Zatsarinny, K. Bartschat, A. Senftleben, X. Ren, J. Ullrich, and A. Dorn, Phys. Rev. Lett. **110**, 153202 (2013).
[10] A. Cassimi, S. Duponchel, X. Flechard, P. Jardin, P. Sortais, D. Hennecart, and R. E. Olson, Phys. Rev. Lett. **76**, 3679 (1996).
[11] M. Abdallah, C.L. Cocke, S. Kravis, E. C. Montenegro, R. Moshammer, L. Saleh, J. Ullrich, S. L. Varghese, W. Wolff, and H. Wolf, Appl. Accel. Res. Ind. AIP Conf. Proc. **392**, 209 (1997).
[12] X. L. Zhu *et al*, Chin. Phys. Lett. **23**, 587 (2006).
[13] M. Alessi, S. Otranto, and P. Focke, Phys. Rev. A **83**, 014701 (2011).
[14] J. Colgan, M. Foster, M. S. Pindzola, I. Bray, A. T. Stelbovics and D. V. Fursa, J. Phys. B: At. Mol. Opt. Phys **42**, 145002 (2009).
[15] I. Bray, D. V. Fursa, A. S. Kadyrov, and A. T. Stelbovics, Phys. Rev. A **81**, 062704 (2010).
[16] M. Dürr, C. Dimopoulou, A. Dorn, B. Najjari, I. Bray, D. V. Fursa, Z. Chen, D. H. Madison, K. Bartschat, and J. Ullrich, J. Phys. B: At. Mol. Opt. Phys. **39**, 4097 (2006).
[17] S. D. Loch, C. J. Favreau and M. S. Pindzola, J. Phys. B: At. Mol. Opt. Phys. **52**, 055205 (2019).
[18] M. S. Pindzola and S. D. Loch, J. Phys. B: At. Mol. Opt. Phys. **52**, 245205 (2019).
[19] C. Granados-Castro and L. U. Ancarani, Eur. Phys. J. D **71**, 65 (2017).
[20] M. Brauner, J. S. Briggs, and H. Klar, J. Phys. B: At. Mol. Opt. Phys. **22**, 2265 (1989).
[21] S. Jones and D. H. Madison, Phys. Rev. Lett. **81**, 2886 (1998).
[22] S. Jones and D. H. Madison, Phys. Rev. A **62**, 042701 (2000).
[23] S. Otranto, Phys. Rev. A **79**, 012705 (2009).
[24] S. Otranto and R. E. Olson, Phys. Rev. A **80**, 012714 (2009).
[25] O. G. de Lucio, S. Otranto, R. E. Olson and R. D. DuBois, Phys. Rev. Lett. **104**, 163201 (2010).
[26] C. Dal Cappello, A. Haddadou, F. Menas, and A. C. Roy, J. Phys. B: At. Mol. Opt. Phys. **44**, 015204 (2011).
[27] D. H. Madison and O. Al-Hagan, J. At. Mol. Opt. Phys. **2010**, 367180 (2010).
[28] S. B. Zhang, X. Y. Li, J. G. Wang, Y. Z. Qu, and X. Chen, Phys. Rev. A **89**, 052711 (2014).
[29] M. Gong, X. Li, S. B. Zhang, S. Niu, X. Ren, E. Wang, A. Dorn, and X. Chen, Phys. Rev. A **98**, 042710 (2018).
[30] E. Ali, C. Granados, A. Sakaamini, M. Harvey, L. U. Ancarani, A. J. Murray, M. Dogan, C. Ning, J. Colgan and D. Madison, J. Chem. Phys. **150**, 194302 (2019).

[31] B. Joulakian, J. Hanssen, R. Rivarola and A. Motassim, Phys. Rev. A **54**, 1473 (1996).

[32] O. Chuluunbaatar, B. Joulakian, K. Tsookhuu and S. I. Vinitsky, J. Phys. B: At. Mol. Opt. Phys. **37**, 2607 (2004).

[33] O. Chuluunbaatar and B. Joulakian, J. Phys. B: At. Mol. Opt. Phys. **43**, 155201 (2010).

[34] S. J. Ward and J. H. Macek, Phys. Rev. A **49**, 1049 (1994).

[35] E. Ali and D. H. Madison, Phys. Rev. A **100**, 012712 (2019).

[36] E. Acebal and S. Otranto, Phys. Rev. A **98**, 012703 (2018).

[37] D. S. F. Crothers and J. S. McCaan, J. Phys. B: At. Mol. Phys. **16** 3229 (1983).

[38] P. D. Fainstein, V. H. Ponce and R. D. Rivarola, J. Phys. B: At. Mol. Opt. Phys. **34**, 3091 (1991).

[39] M. Fiori, A. B. Rocha, C. E. Bielschowsky, G. Jalbert, and C. R. Garibotti, J. Phys. B: At. Mol. Opt. Phys. **39**, 1751 (2006).

[40] J. E. Miraglia, Phys. Rev. A **79**, 022708 (2009).

[41] S. Bhattacharjee, S. Biswas, J. M. Monti, R. D. Rivarola and L. C. Tribedi, Phys. Rev. A **96** 052707 (2017).

[42] X. Ren, T. Pflüger, S. Xu, J. Colgan, M. S. Pindzola, A. Senftleben, J. Ullrich, and A. Dorn, Phys. Rev. Lett. **109**, 123202 (2012).

[43] M. S. Pindzola, F. Robicheaux, S.D. Loch and J. P. Colgan, Phys. Rev. A **73**, 052706 (2006).

[44] E. Acebal and S. Otranto, Eur. Phys. J. D, **73**, 91 (2019).

[45] G. M. J. Barca, C. Bertoni, L. Carrington, D. Datta, N. De Silva, J. E. Deustua, D. G. Fedorov, J. R. Gour, A. O. Gunina, E. Guidez, T. Harville, S. Irle, J. Ivanic, K. Kowalski, S. S. Leang, H. Li, W. Li, J. J. Lutz, I. Magoulas, J. Mato, V. Mironov, H. Nakata, B. Q. Pham, P. Piecuch, D. Poole, S. R. Pruitt, A. P. Rendell, L. B. Roskop, K. Ruedenberg, T. Sattasathuchana, M. W. Schmidt, J. Shen, L. Slipchenko, M. Sosonkina, V. Sundriyal, A. Tiwari, J. L. Galvez Vallejo, B. Westheimer, M. Włoch, P. Xu, F. Zahariev, and M. S. Gordon, J. Chem. Phys. **152**, 154102 (2020). Version: 2019 R1.

[46] L. Fernández-Menchero and S. Otranto, Phys. Rev. A **82**, 022712 (2010).

[47] L. Fernández-Menchero and S. Otranto, J. Phys. B: At. Mol. Opt. Phys. **47**, 035205 (2014).

[48] N. Bachi, S. Otranto, G. S. Otero, and R. E. Olson, Phys. Med. Biol. **64**, 205020 (2019).

[49] A. Senftleben, T Pflüger, X. Ren, B. Najjari, A. Dorn and J. Ullrich, J. Phys. B: At. Mol. Opt. Phys. **45**, 021001 (2012).

[50] F. Salvat, J. M. Fernández-Varea, and W. Williamson, J. Comput. Phys. Commun. **90** 151 (1995).

[51] T. Hahn, Comput. Phys. Comm. **168**, 78 (2005).

[52] A. W. Malcherek and J. S. Briggs, J. Phys. B: At. Mol. Opt. Phys **30** 4419 (1997).

[53] L. D. Landau and E. M. Lifshitz, *Quantum Mechanichs Non-Relativistic Theory*, Pergamon Press, Oxford (1977).

[54] C. J. Wood and R. E. Olson, Phys. Rev. A **59**, 1317 (1999).

[55] M. Alessi, N. D. Cariatore, P. Focke and S. Otranto, Phys. Rev. A **85**, 042704 (2012).

[56] J. E. Miraglia, M. G. Bustamante and P. A. Macri, Phys. Rev. A **60** 4532 (1999).

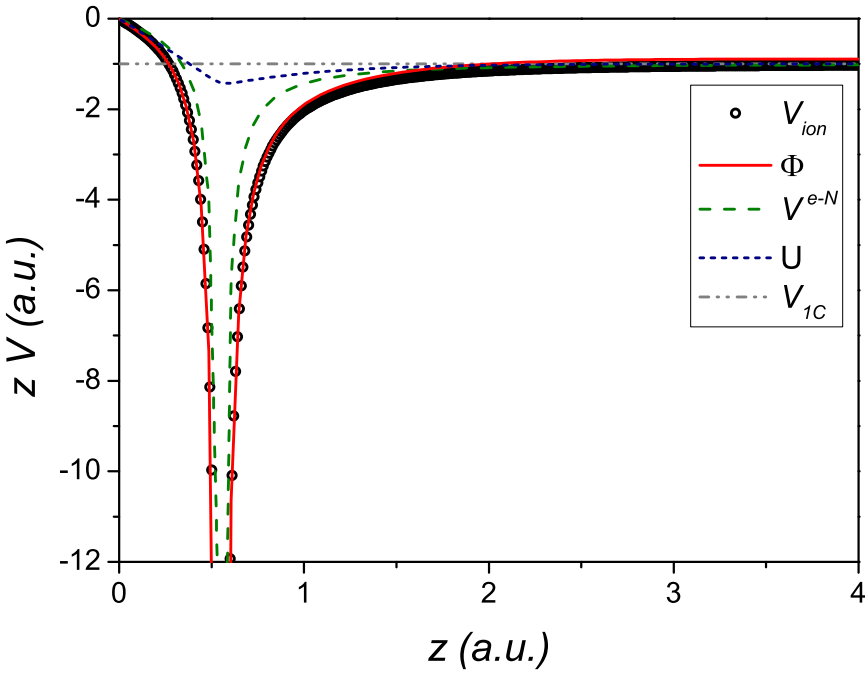

FIG. 1. Approximations to the H_2^+ ion residual potential for a continuum state electron.

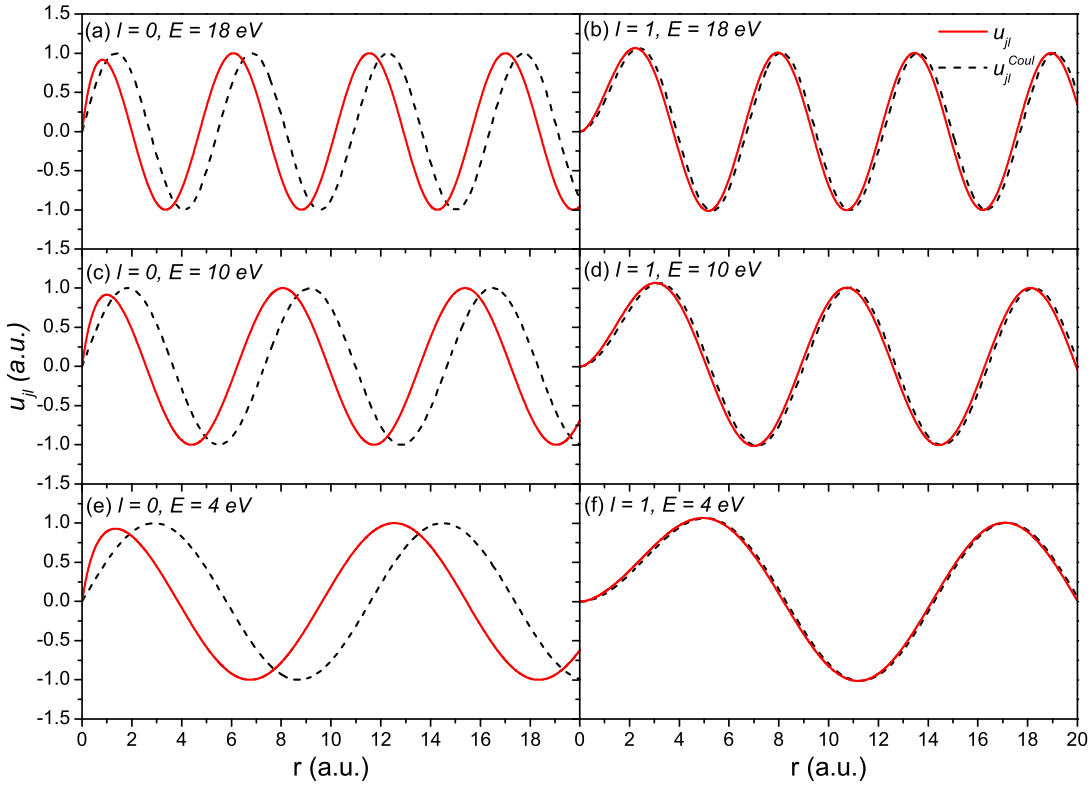

FIG. 2. Partial waves $u_{jl}(k,r)$ (solid lines) and $u_{jl}^{Coul}(k,r)$ (dashed lines) for $l = 0-1$ for continuum electron energies of 4 eV, 10 eV and 18 eV.

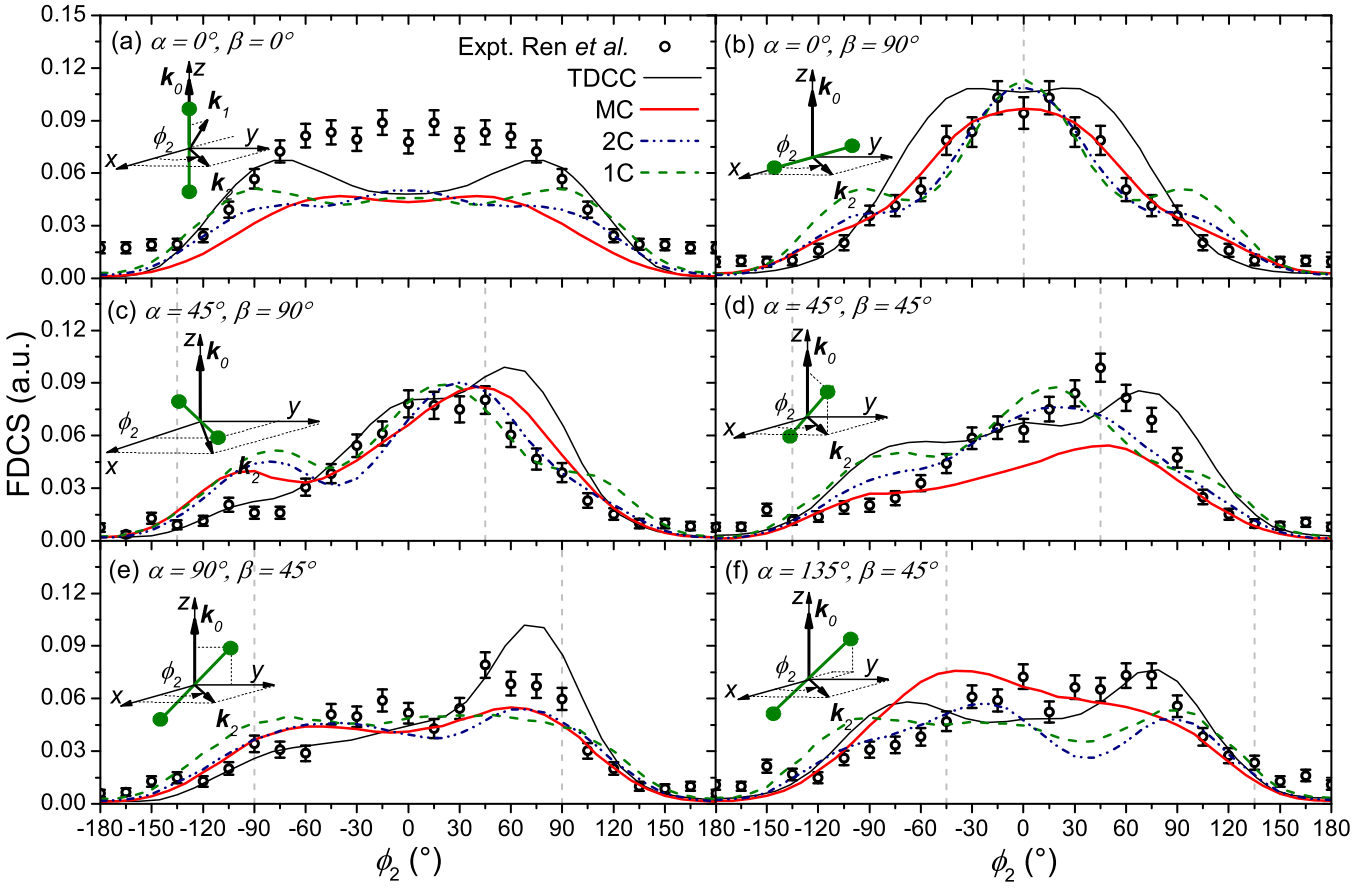

FIG. 3. Fully differential cross sections for the 54 eV electron-impact ionization of aligned H_2 molecules and equal energy sharing ($E_1 = E_2 = 18$ eV) with one electron emission angle fixed at $\theta_1 = -50°$ [$\mathbf{k}_1$ indicated in (a)] as a function of the emission angle of the second electron into the perpendicular xy plane. The light-grey dashed vertical lines indicate the direction of the atoms positions or their projections to the xy plane. The experimental and theoretical data from Ref. [42] are scaled to the present theoretical results.

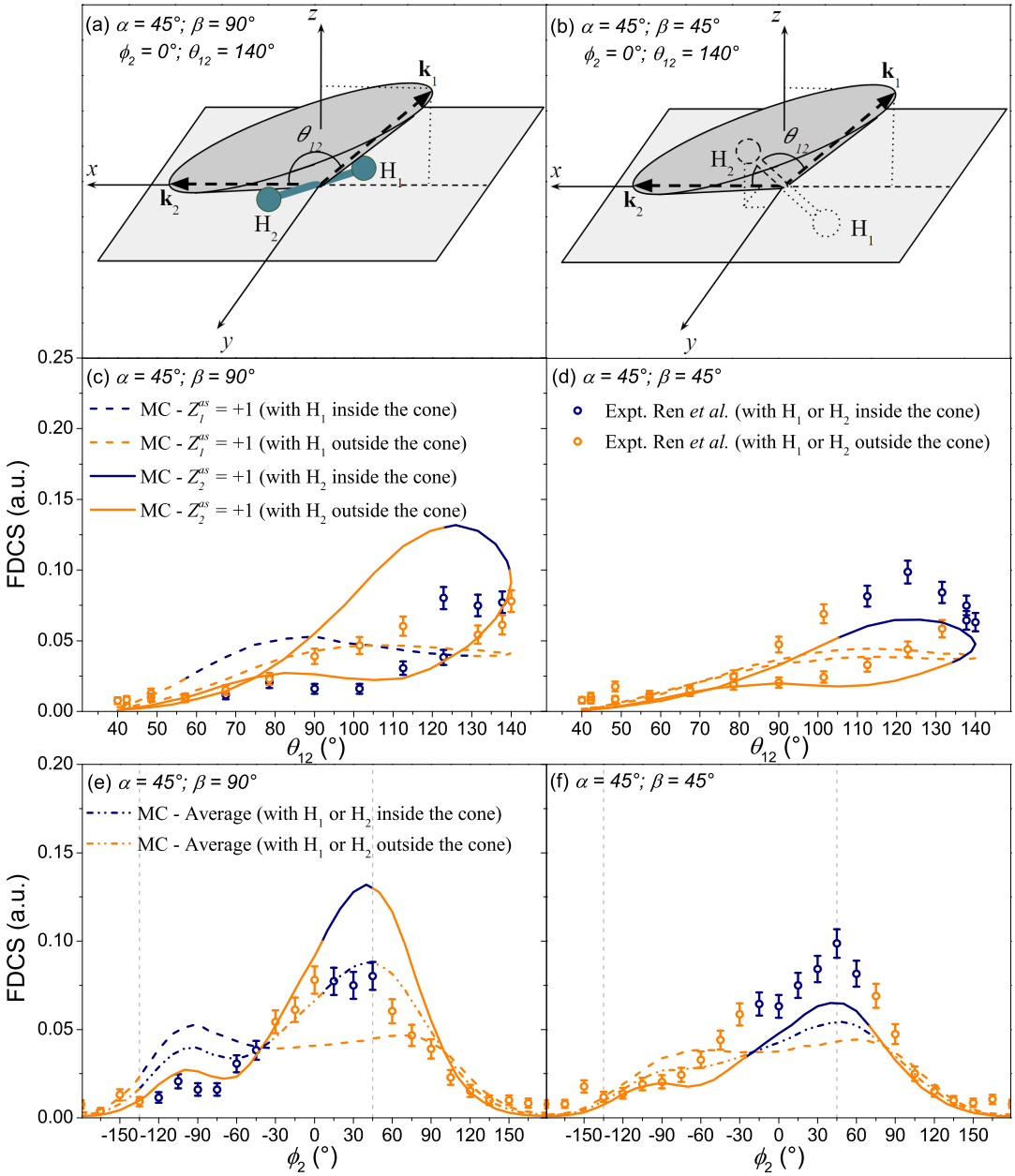

FIG. 4. Same as Fig. 3 for the MC-CDW-EIS model for two different molecular orientations: $(\alpha = 45°, \beta = 90°)$ in the left column and $(\alpha = 45°, \beta = 45°)$ in the right column as a function of the angle θ_{12} between the continuum electron momenta $\mathbf{k}_1$ and $\mathbf{k}_2$ (center panel) and the emission angle ϕ_2 (bottom panel). Graphical representations of these two emission geometries for the particular case $\phi_2 = 0°$ are shown in panels (a) and (b).

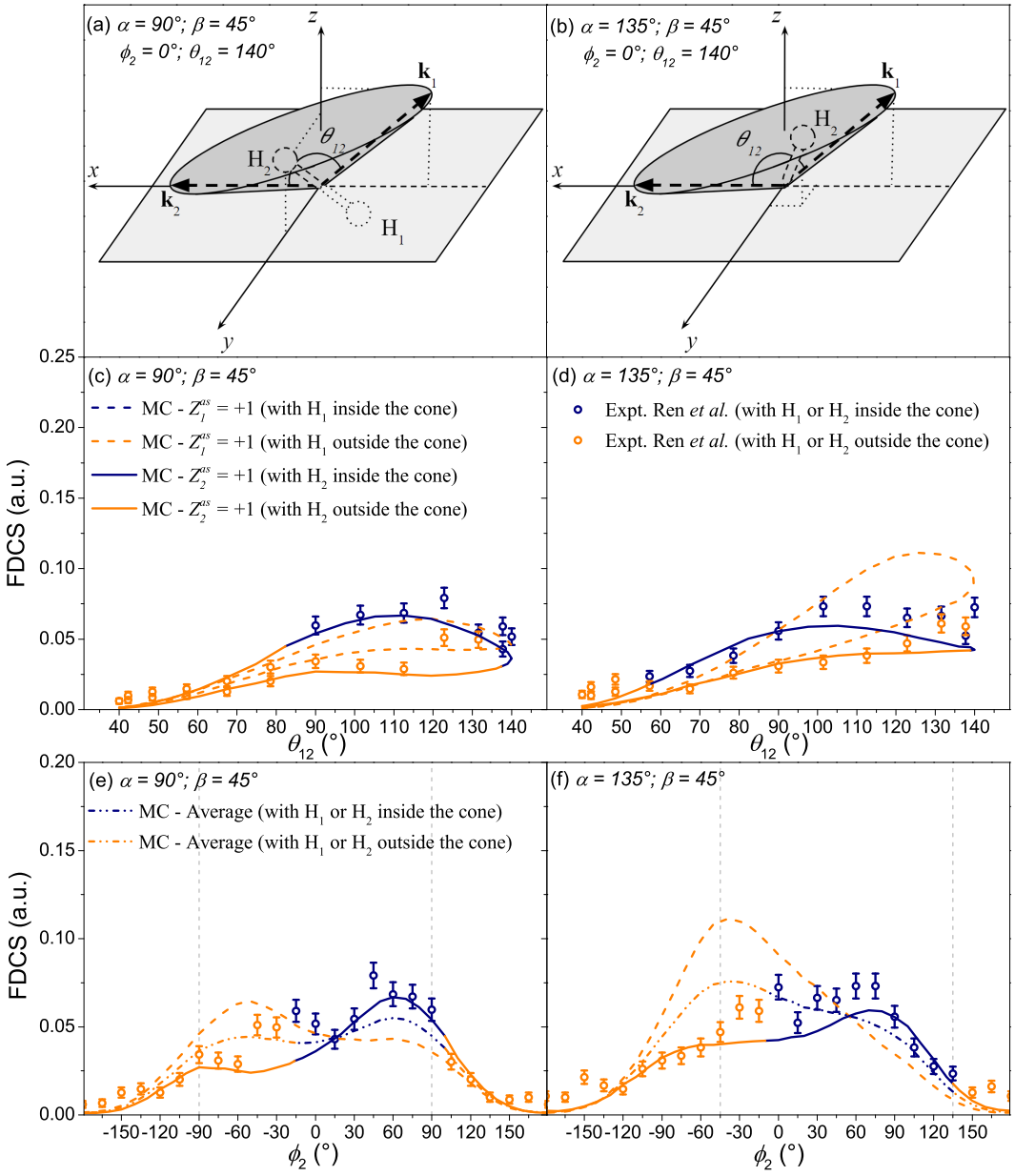

FIG. 5. Same as Fig. 4 for two other molecular orientations: $(\alpha = 90°, \beta = 45°)$ (left column) and $(\alpha = 135°, \beta = 45°)$ (right column).

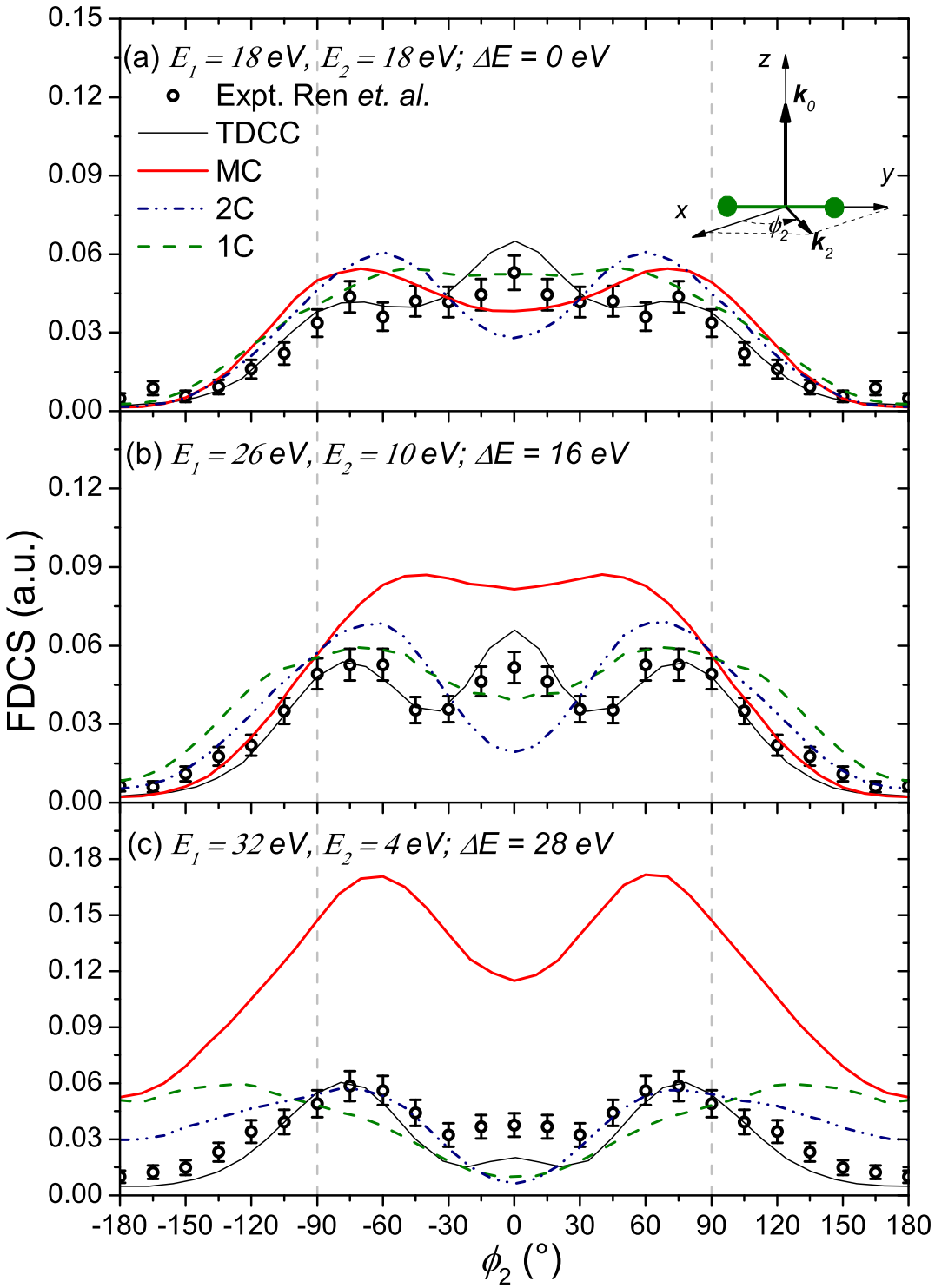

FIG. 6. Same as Fig. 3 with the H_2 molecule aligned along the y-axis and for variable-energy sharing. Emission energies are indicated in the insets.